

Fig. 2. Operating mechanism of the LDC power chain.

processing unit, a sensor unit, and a power management unit shown in gray solid lines. The link evaluation should have minimal disturbance on the original system functionality, and the outputs are preferred in digital. To achieve these goals, a non-inverting buck-boost power chain and a multi-resolution counting analog-to-digital converter (ADC) have been adopted in the proposed LDC.

The buck-boost chain consists of switches (M1, M2, M3, and M4), an inductor (L), and a hysteresis comparator. When C_{IN} is charged beyond the hysteresis comparator turn-on threshold voltage, Phase I begins as shown in Fig. 2. During Phase I, the comparator closes M1 and M3, and some of the charges in C_{IN} are discharged through L. As L gets energized, C_{IN} loses its charges, and V_{IN} decreases. When V_{IN} is below the turn-off threshold voltage, the comparator opens up M1 and M3 and closes M2 and M4 (the beginning of Phase II). During Phase II, the previously energized L dumps its remaining magnetic charge to C_{AUX} . When V_{IN} charges up beyond the switching threshold, Phase II ends, and Phase I repeats.

As link variations influence the charge flow rate in C_{IN} , the buck-boost chain translates the charge flow rate into a ratio of a Phase I duration, t_{on} , to a Phase II duration, t_{off} ; since the charge injection originates from the voltage multiplier, the sum of the two duration stays constant. From the principle of inductor volt-second balance [6], we can see that V_{AUX} is strongly correlated with link-variations

$$\frac{V_{IN}t_{on}}{L} = \frac{V_{AUX}t_{off}}{L} \rightarrow V_{AUX} = \frac{t_{on}}{t_{off}} V_{IN} = \frac{D}{1-D} V_{IN} \quad (1)$$

where $D = t_{on}/(t_{on}+t_{off})$ and V_{IN} is proportional to the charge flow rate.

The digitizer in the LDC is realized with a ring oscillator and a digital counter. The supply of the oscillator, which consists of eight inverters and a NAND for an enable function, is connected to V_{AUX} . The oscillation frequency is proportional to V_{AUX} , and the counter converts the frequency into a digital code that represents the strength of V_{AUX} . The counting duration is controlled

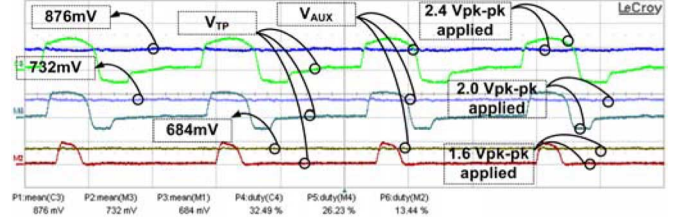


Fig. 3. Duty cycles and power chain output voltages for 2 MHz input AC amplitudes of 2.4, 2.0, and 1.6 Vpk-pk applied to the power receiver.

by the width of a pulse from the pulse generator. This duration determines how much energy should be invested for the link-evaluation; a longer period of counting can result in a finer resolution.

III. TUNABLE POWER RECEIVER PROTOTYPE

The tunable power receiver prototype consists of an off-chip tunable L-C network, a three-stage rectifier, and a proposed LDC block. The L-C network is realized with a flexible printed circuit board (FPCB) inductor and film-trim capacitors. The FPCB inductor was designed to have Q-factor above 100 and inductance of 15 μH . The physical dimension of the FPCB inductor is about 45 mm \times 45 mm. For the prototype verification, the same FPCB inductors are used for the primary and the secondary coils. The three-stage rectifier is implemented with diode-connected transistors and forms the main energy path.

The amount of dc energy harvested at C3 will be affected by the link-variations in the inductively coupled link; mismatches in the resonant matching networks and inductor misalignments would be major cause for the link-variations. Therefore, with the power receiver prototype, realistic link-variations can be emulated and the functionality of the proposed LDC can be tested. Since the buck-boost power chain in the LDC isolates the remaining evaluation blocks from the main energy path, the input energy can be continuously harvested even during the link-evaluation. After the evaluation, the LDC is disabled, and the evaluation results are applied to the link-tuning operation in which a simple binary algorithm adjusts the off-chip tunable capacitor banks.

IV. MEASUREMENTS

The combination of the FPCB inductors and the capacitor banks has a resonant frequency range of 1–5 MHz. Fig. 3 shows the power chain output, V_{AUX} , and the corresponding duty cycle waveforms, V_{TP} , for three input amplitudes, 2.4 V_{pk-pk}, 2.0 V_{pk-pk}, and 1.6 V_{pk-pk}, applied to the prototype. As 2 MHz signals are applied to the receiver with pulse periods of 2.5 μs , 5 μs , and 10 μs , the rectifier output, V_{RECT} , and the LDC outputs are plotted in Fig. 4. The higher counting period is, the finer input amplitude can be differentiated.

To verify the link-evaluation capability under component mismatches, a 2 MHz signal is transmitted through a fixed primary resonant network to a 2 mm-away secondary resonant network, and the rectifier voltages and the LDC outputs are measured with various tuning capacitor values in Fig. 5. To emulate realistic inductor misalignment situations, the proposed

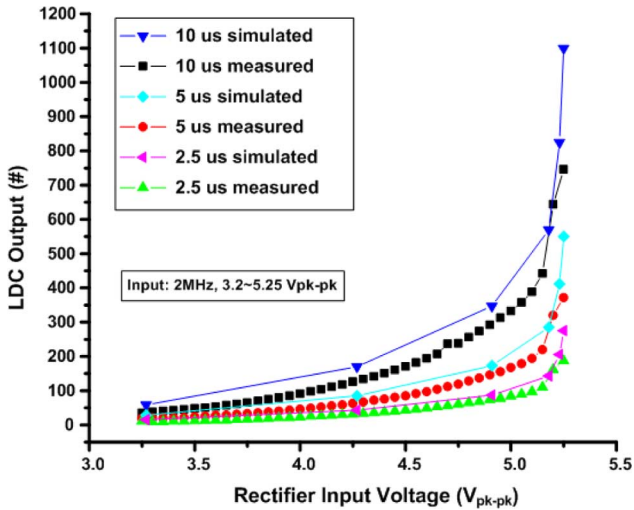


Fig. 4. LDC outputs when 2 MHz sinusoidal signals with 3.2–5.25 V_{pk-pk} are applied to the input of the rectifier.

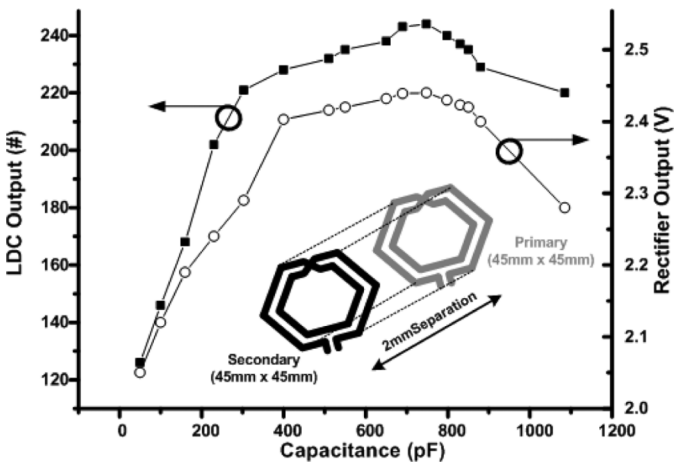


Fig. 5. Tuning capacitance value versus LDC digital outputs and corresponding rectifier output voltages.

power receiver was tested with five different inductor alignments. While the coordinate of the primary inductor is fixed, the secondary inductor is offset by 2 mm distance in either/both X -direction and Y -direction. For the inductor misalignments, the LDC outputs are measured with various capacitor values, as shown in Fig. 6.

The active area of the prototype, implemented in CMOS $0.18 \mu\text{m}$, is $500 \mu\text{m}$ -by- $250 \mu\text{m}$. Fig. 7 shows the die photo of the prototype and an inductor misalignment that has been tested.

V. CONCLUSION

In practical wireless sensor applications, unpredictable variations in the wireless link inevitably degrade the overall system performance. Evaluating the link variations in real-time is highly desirable for more reliable and efficient operations. This work presents a unique non-interruptive link-variation sensing technique that can provide *in situ* multi-resolution assessments.

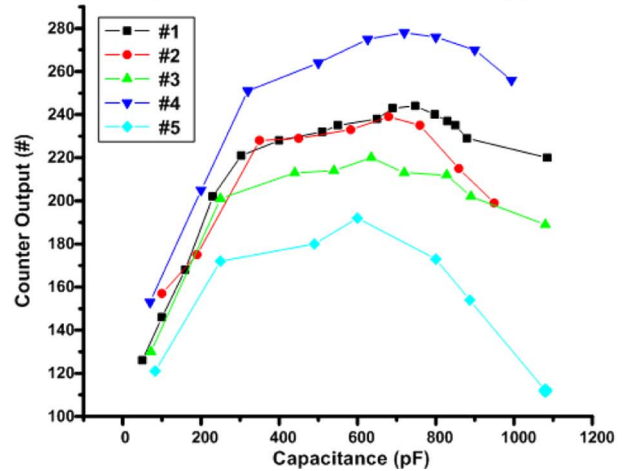
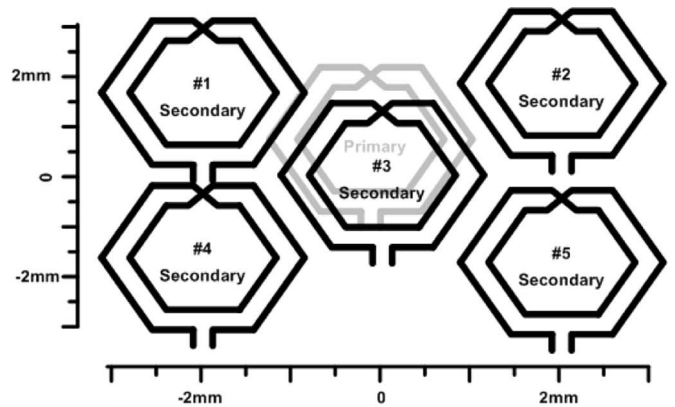


Fig. 6. Tuning capacitance value versus LDC digital outputs under various inductor misalignments.

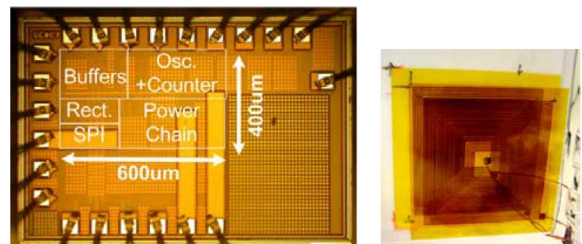


Fig. 7. Die micrograph of the power receiver prototype and an example of an inductor misalignment.

REFERENCES

- [1] I. F. Akyildiz, W. Su, and Y. Sankarasubramaniam, “Wireless sensor networks: A survey,” *Comp. Netw.*, vol. 38, pp. 393–422, 2002.
- [2] B. W. Cook, S. Lanzisera, and K. S. J. Pister, “SoC issues for RF smart dust,” *Proc. IEEE*, vol. 94, no. 6, pp. 1177–1196, Jun. 2006.
- [3] J. Yoo, S. Lee, and H.-J. Yoo, “A 1.12 pJ/b inductive transceiver with a fault-tolerant network switch from multi-layer wearable body area network applications,” *IEEE J. Solid-State Circuits*, vol. 44, no. 11, pp. 2999–3010, Nov. 2009.
- [4] S. Lee, J. Yoo, H. Kim, and H.-J. Yoo, “A dynamic real-time capacitor compensated inductive coupling transceiver for wearable body sensor network,” in *Symp. VLSI Circuits Dig. Tech. Papers*, Jun. 2009, pp. 42–43.
- [5] S. O’Driscoll, A. Poon, and T. H. Meng, “A mm-sized implantable power receiver with adaptive link compensation,” in *IEEE ISSCC Dig. Tech. Papers*, Feb. 2009, pp. 294–295.
- [6] R. W. Erickson and D. Maksimovic, *Fundamentals of Power Electronics*, 2nd ed. Norwell, MA: Kluwer, 2001, pp. 13–35.